

Measurements of isospin asymmetry and difference of direct CP asymmetries in inclusive $B \rightarrow X_s \gamma$ decays

S. Watanuki,⁸² A. Ishikawa,⁸² I. Adachi,^{17,14} H. Aihara,⁸⁴ S. Al Said,^{78,36} D. M. Asner,⁴
 T. Aushev,⁵⁴ R. Ayad,⁷⁸ V. Babu,⁷⁹ I. Badhrees,^{78,35} A. M. Bakich,⁷⁷ V. Bansal,⁶⁷
 P. Behera,²⁴ C. Beleño,¹³ M. Berger,⁷⁵ V. Bhardwaj,²¹ B. Bhuyan,²² T. Bilka,⁶ J. Biswal,³²
 A. Bobrov,^{5,65} G. Bonvicini,⁸⁸ A. Bozek,⁶¹ M. Bračko,^{48,32} T. E. Browder,¹⁶ L. Cao,³⁴
 D. Červenkov,⁶ P. Chang,⁶⁰ B. G. Cheon,¹⁵ K. Chilikin,⁴⁴ K. Cho,³⁸ Y. Choi,⁷⁶
 S. Choudhury,²³ D. Cinabro,⁸⁸ S. Cunliffe,⁹ S. Di Carlo,⁴² J. Dingfelder,³ T. V. Dong,^{17,14}
 S. Eidelman,^{5,65,44} D. Epifanov,^{5,65} J. E. Fast,⁶⁷ T. Ferber,⁹ A. Frey,¹³ B. G. Fulsom,⁶⁷
 V. Gaur,⁸⁷ N. Gabyshev,^{5,65} A. Garmash,^{5,65} M. Gelb,³⁴ A. Giri,²³ P. Goldenzweig,³⁴
 Y. Guan,^{25,17} E. Guido,³⁰ J. Haba,^{17,14} K. Hayasaka,⁶³ H. Hayashii,⁵⁸ W.-S. Hou,⁶⁰
 T. Iijima,^{56,55} K. Inami,⁵⁵ G. Inguglia,⁹ R. Itoh,^{17,14} M. Iwasaki,⁶⁶ Y. Iwasaki,¹⁷
 W. W. Jacobs,²⁵ I. Jaegle,¹¹ H. B. Jeon,⁴¹ S. Jia,² Y. Jin,⁸⁴ K. K. Joo,⁷ T. Julius,⁵⁰
 G. Karyan,⁹ T. Kawasaki,³⁷ C. Kiesling,⁴⁹ D. Y. Kim,⁷⁴ J. B. Kim,³⁹ S. H. Kim,¹⁵
 K. Kinoshita,⁸ P. Kodyš,⁶ S. Korpar,^{48,32} D. Kotchetkov,¹⁶ P. Krizán,^{45,32} R. Kroeger,⁵¹
 P. Krokovny,^{5,65} T. Kuhr,⁴⁶ R. Kumar,⁷⁰ A. Kuzmin,^{5,65} Y.-J. Kwon,⁹⁰ I. S. Lee,¹⁵
 S. C. Lee,⁴¹ L. K. Li,²⁶ Y. B. Li,⁶⁸ L. Li Gioi,⁴⁹ J. Libby,²⁴ D. Liventsev,^{87,17} M. Lubej,³²
 T. Luo,¹² M. Masuda,⁸³ T. Matsuda,⁵² M. Merola,^{29,57} K. Miyabayashi,⁵⁸ H. Miyata,⁶³
 R. Mizuk,^{44,53,54} G. B. Mohanty,⁷⁹ T. Mori,⁵⁵ M. Nakao,^{17,14} T. Nanut,³² K. J. Nath,²²
 M. Niiyama,⁴⁰ S. Nishida,^{17,14} K. Nishimura,¹⁶ K. Ogawa,⁶³ S. Ogawa,⁸¹ S. Okuno,³³
 H. Ono,^{62,63} W. Ostrowicz,⁶¹ P. Pakhlov,^{44,53} G. Pakhlova,^{44,54} B. Pal,⁴ H. Park,⁴¹
 S. Paul,⁸⁰ T. K. Pedlar,⁴⁷ R. Pestotnik,³² L. E. Piilonen,⁸⁷ E. Prencipe,¹⁹ M. Ritter,⁴⁶
 A. Rostomyan,⁹ G. Russo,²⁹ Y. Sakai,^{17,14} S. Sandilya,⁸ L. Santelj,³² V. Savinov,⁶⁹
 O. Schneider,⁴³ G. Schnell,^{1,20} J. Schueler,¹⁶ C. Schwanda,²⁷ A. J. Schwartz,⁸ Y. Seino,⁶³
 K. Senyo,⁸⁹ O. Seon,⁵⁵ V. Shebalin,^{5,65} T.-A. Shibata,⁸⁵ J.-G. Shiu,⁶⁰ B. Shwartz,^{5,65}
 A. Sokolov,²⁸ E. Solovieva,^{44,54} S. Stanič,⁶⁴ M. Starič,³² T. Sumiyoshi,⁸⁶ W. Sutcliffe,³⁴
 M. Takizawa,^{73,18,71} K. Tanida,³¹ N. Taniguchi,¹⁷ F. Tenchini,⁹ M. Uchida,⁸⁵ T. Uglov,^{44,54}
 Y. Unno,¹⁵ S. Uno,^{17,14} S. E. Vahsen,¹⁶ C. Van Hulse,¹ R. Van Tonder,³⁴ G. Varner,¹⁶
 K. E. Varvell,⁷⁷ A. Vossen,¹⁰ B. Wang,⁸ C. H. Wang,⁵⁹ M.-Z. Wang,⁶⁰ P. Wang,²⁶
 M. Watanabe,⁶³ E. Widmann,⁷⁵ E. Won,³⁹ H. Ye,⁹ J. H. Yin,²⁶ Y. Yusa,⁶³ S. Zakharov,^{44,54}
 Z. P. Zhang,⁷² V. Zhilich,^{5,65} V. Zhukova,^{44,53} V. Zhulanov,^{5,65} and A. Zupanc^{45,32}

(The Belle Collaboration)

¹University of the Basque Country UPV/EHU, 48080 Bilbao

²Beihang University, Beijing 100191

³University of Bonn, 53115 Bonn

⁴Brookhaven National Laboratory, Upton, New York 11973

⁵Budker Institute of Nuclear Physics SB RAS, Novosibirsk 630090

⁶Faculty of Mathematics and Physics, Charles University, 121 16 Prague

⁷Chonnam National University, Kwangju 660-701

- ⁸University of Cincinnati, Cincinnati, Ohio 45221
- ⁹Deutsches Elektronen-Synchrotron, 22607 Hamburg
- ¹⁰Duke University, Durham, North Carolina 27708
- ¹¹University of Florida, Gainesville, Florida 32611
- ¹²Key Laboratory of Nuclear Physics and Ion-beam Application (MOE) and Institute of Modern Physics, Fudan University, Shanghai 200443
- ¹³II. Physikalisches Institut, Georg-August-Universität Göttingen, 37073 Göttingen
- ¹⁴SOKENDAI (The Graduate University for Advanced Studies), Hayama 240-0193
- ¹⁵Hanyang University, Seoul 133-791
- ¹⁶University of Hawaii, Honolulu, Hawaii 96822
- ¹⁷High Energy Accelerator Research Organization (KEK), Tsukuba 305-0801
- ¹⁸J-PARC Branch, KEK Theory Center, High Energy Accelerator Research Organization (KEK), Tsukuba 305-0801
- ¹⁹Forschungszentrum Jülich, 52425 Jülich
- ²⁰IKERBASQUE, Basque Foundation for Science, 48013 Bilbao
- ²¹Indian Institute of Science Education and Research Mohali, SAS Nagar, 140306
- ²²Indian Institute of Technology Guwahati, Assam 781039
- ²³Indian Institute of Technology Hyderabad, Telangana 502285
- ²⁴Indian Institute of Technology Madras, Chennai 600036
- ²⁵Indiana University, Bloomington, Indiana 47408
- ²⁶Institute of High Energy Physics, Chinese Academy of Sciences, Beijing 100049
- ²⁷Institute of High Energy Physics, Vienna 1050
- ²⁸Institute for High Energy Physics, Protvino 142281
- ²⁹INFN - Sezione di Napoli, 80126 Napoli
- ³⁰INFN - Sezione di Torino, 10125 Torino
- ³¹Advanced Science Research Center, Japan Atomic Energy Agency, Naka 319-1195
- ³²J. Stefan Institute, 1000 Ljubljana
- ³³Kanagawa University, Yokohama 221-8686
- ³⁴Institut für Experimentelle Teilchenphysik, Karlsruher Institut für Technologie, 76131 Karlsruhe
- ³⁵King Abdulaziz City for Science and Technology, Riyadh 11442
- ³⁶Department of Physics, Faculty of Science, King Abdulaziz University, Jeddah 21589
- ³⁷Kitasato University, Tokyo 108-0072
- ³⁸Korea Institute of Science and Technology Information, Daejeon 305-806
- ³⁹Korea University, Seoul 136-713
- ⁴⁰Kyoto University, Kyoto 606-8502
- ⁴¹Kyungpook National University, Daegu 702-701
- ⁴²LAL, Univ. Paris-Sud, CNRS/IN2P3, Université Paris-Saclay, Orsay
- ⁴³École Polytechnique Fédérale de Lausanne (EPFL), Lausanne 1015
- ⁴⁴P.N. Lebedev Physical Institute of the Russian Academy of Sciences, Moscow 119991
- ⁴⁵Faculty of Mathematics and Physics, University of Ljubljana, 1000 Ljubljana
- ⁴⁶Ludwig Maximilians University, 80539 Munich

- ⁴⁷*Luther College, Decorah, Iowa 52101*
- ⁴⁸*University of Maribor, 2000 Maribor*
- ⁴⁹*Max-Planck-Institut für Physik, 80805 München*
- ⁵⁰*School of Physics, University of Melbourne, Victoria 3010*
- ⁵¹*University of Mississippi, University, Mississippi 38677*
- ⁵²*University of Miyazaki, Miyazaki 889-2192*
- ⁵³*Moscow Physical Engineering Institute, Moscow 115409*
- ⁵⁴*Moscow Institute of Physics and Technology, Moscow Region 141700*
- ⁵⁵*Graduate School of Science, Nagoya University, Nagoya 464-8602*
- ⁵⁶*Kobayashi-Maskawa Institute, Nagoya University, Nagoya 464-8602*
- ⁵⁷*Università di Napoli Federico II, 80055 Napoli*
- ⁵⁸*Nara Women's University, Nara 630-8506*
- ⁵⁹*National United University, Miao Li 36003*
- ⁶⁰*Department of Physics, National Taiwan University, Taipei 10617*
- ⁶¹*H. Niewodniczanski Institute of Nuclear Physics, Krakow 31-342*
- ⁶²*Nippon Dental University, Niigata 951-8580*
- ⁶³*Niigata University, Niigata 950-2181*
- ⁶⁴*University of Nova Gorica, 5000 Nova Gorica*
- ⁶⁵*Novosibirsk State University, Novosibirsk 630090*
- ⁶⁶*Osaka City University, Osaka 558-8585*
- ⁶⁷*Pacific Northwest National Laboratory, Richland, Washington 99352*
- ⁶⁸*Peking University, Beijing 100871*
- ⁶⁹*University of Pittsburgh, Pittsburgh, Pennsylvania 15260*
- ⁷⁰*Punjab Agricultural University, Ludhiana 141004*
- ⁷¹*Theoretical Research Division, Nishina Center, RIKEN, Saitama 351-0198*
- ⁷²*University of Science and Technology of China, Hefei 230026*
- ⁷³*Showa Pharmaceutical University, Tokyo 194-8543*
- ⁷⁴*Soongsil University, Seoul 156-743*
- ⁷⁵*Stefan Meyer Institute for Subatomic Physics, Vienna 1090*
- ⁷⁶*Sungkyunkwan University, Suwon 440-746*
- ⁷⁷*School of Physics, University of Sydney, New South Wales 2006*
- ⁷⁸*Department of Physics, Faculty of Science, University of Tabuk, Tabuk 71451*
- ⁷⁹*Tata Institute of Fundamental Research, Mumbai 400005*
- ⁸⁰*Department of Physics, Technische Universität München, 85748 Garching*
- ⁸¹*Toho University, Funabashi 274-8510*
- ⁸²*Department of Physics, Tohoku University, Sendai 980-8578*
- ⁸³*Earthquake Research Institute, University of Tokyo, Tokyo 113-0032*
- ⁸⁴*Department of Physics, University of Tokyo, Tokyo 113-0033*
- ⁸⁵*Tokyo Institute of Technology, Tokyo 152-8550*
- ⁸⁶*Tokyo Metropolitan University, Tokyo 192-0397*
- ⁸⁷*Virginia Polytechnic Institute and State University, Blacksburg, Virginia 24061*
- ⁸⁸*Wayne State University, Detroit, Michigan 48202*
- ⁸⁹*Yamagata University, Yamagata 990-8560*
- ⁹⁰*Yonsei University, Seoul 120-749*

Abstract

We report measurements of isospin asymmetry Δ_{0-} and difference of direct CP asymmetries ΔA_{CP} between charged and neutral $B \rightarrow X_s \gamma$ decays. This analysis is based on the data sample containing $772 \times 10^6 B \bar{B}$ pairs that was collected with the Belle detector at the KEKB energy-asymmetric e^+e^- collider. Using a sum-of-exclusive technique with invariant X_s mass up to $2.8 \text{ GeV}/c^2$, we obtain $\Delta_{0-} = [-0.48 \pm 1.49(\text{stat.}) \pm 0.97(\text{syst.}) \pm 1.15(f_{+-}/f_{00})]\%$ and $\Delta A_{CP} = [+3.69 \pm 2.65(\text{stat.}) \pm 0.76(\text{syst.})]\%$, where the last uncertainty for Δ_{0-} is due to the uncertainty on the production ratio of B^+B^- to $B^0\bar{B}^0$ in $\Upsilon(4S)$ decays. The measured value of Δ_{0-} is consistent with zero, allowing us to constrain the resolved photon contribution in the $B \rightarrow X_s \gamma$, and improve the branching fraction prediction. The result for ΔA_{CP} is consistent with the prediction of the SM. We also measure the direct CP asymmetries for charged and neutral $B \rightarrow X_s \gamma$ decays. All the measurements are the most precise to date.

PACS numbers: 13.25.Hw, 13.30.Ce, 13.40.Hq, 14.40.Nd

I. INTRODUCTION

The radiative $b \rightarrow s\gamma$ decay proceeds predominantly via one-loop electromagnetic penguin diagrams at the lowest order in the standard model (SM). This decay is sensitive to new physics (NP), which can alter the branching fraction, or direct CP asymmetry defined as

$$A_{CP} = \frac{\Gamma(\bar{B} \rightarrow \bar{X}_s\gamma) - \Gamma(B \rightarrow X_s\gamma)}{\Gamma(\bar{B} \rightarrow \bar{X}_s\gamma) + \Gamma(B \rightarrow X_s\gamma)}, \quad (1)$$

where Γ denotes the partial width.

Precision measurements of $B \rightarrow X_s\gamma$ branching fraction $\mathcal{B}(B \rightarrow X_s\gamma)$ [1–6] are in good agreement with the SM prediction [7] and set a strong constraint on NP models [8]. The theoretical uncertainty in the prediction of $\mathcal{B}(B \rightarrow X_s\gamma)$ is about 7% which is comparable with the experimental uncertainty of the current world average [9]. The Belle II experiment is expected to measure the branching fraction with a precision of about 3% [10]. Thus, the reduction of the theoretical uncertainty is crucial to further constrain NP models. The largest uncertainty in the theoretical prediction is due to non-perturbative effects, one of which is the resolved photon contributions [11]. Since the resolved photon contribution from a hard gluon and a light quark scattering to the $B \rightarrow X_s\gamma$ branching fraction ($\mathcal{B}_{\text{RP}}^{78}$) depends on the charge of the light quark and can be hence related to the isospin asymmetry in $B \rightarrow X_s\gamma$ (Δ_{0-}) as [11–13]

$$\frac{\mathcal{B}_{\text{RP}}^{78}}{\mathcal{B}} \simeq -\frac{(1 \pm 0.3)}{3} \Delta_{0-}, \quad (2)$$

where the uncertainty of ± 0.3 in the right-hand side is associated with $SU(3)$ flavor-symmetry breaking. The isospin asymmetry is defined as

$$\begin{aligned} \Delta_{0-} &= \frac{\Gamma(\bar{B}^0 \rightarrow X_s^0\gamma) - \Gamma(B^- \rightarrow X_s^-\gamma)}{\Gamma(\bar{B}^0 \rightarrow X_s^0\gamma) + \Gamma(B^- \rightarrow X_s^-\gamma)} \\ &= \frac{\frac{\tau_{B^-}}{\tau_{\bar{B}^0}} \frac{f_{+-}}{f_{00}} N(\bar{B}^0 \rightarrow X_s^0\gamma) - N(B^- \rightarrow X_s^-\gamma)}{\frac{\tau_{B^-}}{\tau_{\bar{B}^0}} \frac{f_{+-}}{f_{00}} N(\bar{B}^0 \rightarrow X_s^0\gamma) + N(B^- \rightarrow X_s^-\gamma)}, \end{aligned} \quad (3)$$

where N is the number of produced signal events including charge-conjugate decays, $\tau_{B^-}/\tau_{\bar{B}^0} = \tau_{B^+}/\tau_{B^0}$ is the lifetime ratio of B^+ to B^0 mesons, f_{+-} and f_{00} are the production ratio of B^+B^- to $B^0\bar{B}^0$ in $\Upsilon(4S)$ decays, respectively. If the measured value of Δ_{0-} is consistent with zero, the resolved photon contribution is small and reducing in the theoretical uncertainty on $\mathcal{B}(B \rightarrow X_s\gamma)$. Recently, evidence for isospin violation in exclusive $B \rightarrow K^*(892)\gamma$ (Δ_{0+}) has been reported [14] where the measured value, $\Delta_{0+} = (+6.2 \pm 1.5 \pm 0.5 \pm 1.2)\%$, is consistent with SM predictions [15–20]. If the isospin asymmetry for the inclusive decays is consistent with this value, the resolved photon contribution to $B \rightarrow X_s\gamma$ decays could be sizable.

The direct CP asymmetry in $B \rightarrow X_s\gamma$ is also a sensitive probe for NP [18, 21–30]. Belle [31] and BaBar [32] measured this quantity, and the current world average $(+1.5 \pm 2.0)\%$ [9] is in agreement and of comparable precision, with the SM prediction, $-0.6\% < A_{CP}^{\text{SM}} < +2.8\%$ [33]. The dominant theoretical uncertainty is due to the limited knowledge of the resolved photon contributions. A newly proposed observable is the difference of the direct CP asymmetries between the charged and neutral B mesons, $\Delta A_{CP} = A_{CP}(B^+ \rightarrow X_s^+\gamma) - A_{CP}(B^0 \rightarrow X_s^0\gamma)$, where terms with large weak phase in the SM cancel out, and only the

spectator-quark-flavor dependent term representing interference between electromagnetic and chromomagnetic dipole operators survives [33]:

$$\begin{aligned}\Delta A_{CP} &= 4\pi^2 \alpha_s \frac{\tilde{\Lambda}_{78}}{m_b} \text{Im}\left(\frac{C_8}{C_7}\right) \\ &\approx 0.12 \left(\frac{\tilde{\Lambda}_{78}}{100 \text{ MeV}}\right) \text{Im}\left(\frac{C_8}{C_7}\right),\end{aligned}\tag{4}$$

where α_s is the strong coupling constant, $\tilde{\Lambda}_{78}$ is the hadronic parameter denoting the interference between electromagnetic and chromomagnetic dipole diagrams, m_b is the bottom quark mass, and C_7 and C_8 are the Wilson coefficients for electromagnetic and chromomagnetic dipole operators, respectively [34]. In the SM, C_7 and C_8 are both real, therefore ΔA_{CP} is zero, but in several NP models ΔA_{CP} can reach the level of 10% in magnitude [33, 35, 36].

BaBar measured Δ_{0-} and ΔA_{CP} using data samples of 81.9 fb^{-1} and 429 fb^{-1} , respectively, as $\Delta_{0-} = (-0.6 \pm 5.8 \pm 0.9 \pm 2.4)\%$ [37] and $\Delta A_{CP} = (+5.0 \pm 3.9 \pm 1.5)\%$ [32], where the first uncertainty is statistical, the second is systematic, and the last one for Δ_{0-} is due to the uncertainty on the fraction of B^+B^- to $B^0\bar{B}^0$ production in $\Upsilon(4S)$ decays. The precisions are limited by statistical uncertainties. Improving these measurements is highly desirable to reduce the theoretical uncertainty of $\mathcal{B}(B \rightarrow X_s\gamma)$ in the SM as well as to search for NP.

In this article, we report first measurements of Δ_{0-} and ΔA_{CP} in inclusive $B \rightarrow X_s\gamma$ at Belle assuming that the two observables have no dependence on decay modes nor on the invariant mass of the X_s system (M_{X_s}). In addition, we present measurements of individual A_{CP} for the charged and neutral decay and their average with $\bar{A}_{CP} = (A_{CP}(B^- \rightarrow X_s\gamma) + A_{CP}(\bar{B}^0 \rightarrow X_s\gamma))/2$. All measurements are based on the full data sample of 711 fb^{-1} , containing $772 \times 10^6 B\bar{B}$ pairs, recorded at the $\Upsilon(4S)$ resonance (on-resonance data) with the Belle detector [38] at the KEKB e^+e^- collider [39]. In addition, the data sample of 89 fb^{-1} accumulated 60 MeV below the $\Upsilon(4S)$ peak (off-resonance data), which is below the $B\bar{B}$ production threshold, is used to provide a background description. The result for $A_{CP}(B \rightarrow X_s\gamma)$ supersedes our previous measurement [31].

II. BELLE DETECTOR

The Belle detector is a large-solid-angle magnetic spectrometer that consists of a silicon vertex detector (SVD), a 50-layer central drift chamber (CDC), an array of aerogel threshold Cherenkov counters (ACC), a barrel-like arrangement of time-of-flight scintillation counters (TOF), and an electromagnetic calorimeter comprised of CsI(Tl) crystals (ECL). All the sub-detectors are located inside a superconducting solenoid coil that provides a 1.5 T magnetic field. An iron flux-return placed outside of the coil is instrumented to detect K_L^0 mesons and muons. The z axis is aligned with the direction opposite the e^+ beam. The detector is described in detail elsewhere [38].

III. MC SIMULATION

The selection is optimized with Monte Carlo (MC) simulation samples. The MC simulation events are generated with EvtGen [40] and the detector simulation is done with

GEANT3 [41]. We generate two types of signal MC simulation samples, according to the X_s mass region: in the region $M_{X_s} < 1.15 \text{ GeV}/c^2$, the X_s system solely consists of $K^*(892)$ while in the region $M_{X_s} > 1.15 \text{ GeV}/c^2$, X_s system is simulated inclusively without any specific resonances, except for $K_2^*(1430)$.

In the inclusive signal MC simulation sample, various resonances and final states are simulated. The photon energy spectrum in this sample is produced following the Kagan-Neubert model [42]. The model has two parameters: the b quark mass (m_b) and the Fermi-motion parameter of the b quark inside the B meson (μ_π^2). The nominal values of these parameters are determined from a fit to the Belle inclusive photon energy spectrum [5]: $m_b = 4.440 \text{ GeV}/c^2$ and $\mu_\pi^2 = 0.750 \text{ GeV}^2$. Further, the generated light quark pair is fragmented into final-state hadrons using PYTHIA [43].

Since the $B \rightarrow K_2^*(1430)\gamma$ decay has a relatively large branching fraction, dedicated MC simulation samples are generated. The decay is generated with the measured branching fraction and then added to the inclusive signal MC simulation sample. To match the photon spectrum with the theoretical one, the M_{X_s} distribution for $K\pi$ and $K2\pi$ modes in the inclusive sample is rescaled. The signal reconstruction efficiency depends on the particle content in the final state; thus, the hadronization of X_s is studied using data. We set the branching fraction of $B \rightarrow X_s\gamma$ to the current world average [9] in order to optimize the background rejection.

IV. EVENT SELECTION

We reconstruct $B \rightarrow X_s\gamma$ decays with 38 exclusive X_s final states listed in Table I. As shown in Table II, we group the final states into ten categories for the purpose of specific selections and fragmentation model calibrations. The reconstructed decay modes cover 59% of the total X_s rate, according to the MC simulations. Assuming the K^0 meson to decay equally into K_L^0 and K_S^0 , the proportion of our measured final states is 77% of the total X_s rate. For neutral B decays, all flavor-specific final states are used for the measurements of both A_{CP} and Δ_{0-} , and 11 flavor-non-specific final states, denoted as B_{fns} , are only used for the measurement of Δ_{0-} .

High-energy prompt photons are selected as isolated clusters in the ECL that are not matched to any charged tracks reconstructed by the SVD and the CDC. The cluster energy in the center of mass (CM) system is required to be between 1.5 and 3.4 GeV. The polar angle of the photon direction must be within the barrel ECL, $33^\circ < \theta < 132^\circ$. We also require the cluster shape to be consistent with an electromagnetic shower, $E_9/E_{25} > 0.95$, where E_9/E_{25} is the ratio of energy deposits in the 3×3 array of CsI(Tl) crystals to that in the 5×5 array centered on the crystal with maximum energy. In order to reduce contaminations from asymmetric $\eta \rightarrow \gamma\gamma$ or $\pi^0 \rightarrow \gamma\gamma$ decays, the photon candidate is paired with all other photons in the event with energy greater than 40 MeV. We reject the pairs based on likelihoods (\mathcal{L}_{π^0} and \mathcal{L}_η), constructed from their invariant mass, and the energy and polar angle of the additional photon in the CM system [45]. The photon candidate which has $\mathcal{L}_{\pi^0} > 0.05$ or $\mathcal{L}_\eta > 0.10$ is discarded.

Charged particles, except pions from K_S^0 decays, are required to have a distance of closest approach to the interaction point (IP) within $\pm 5.0 \text{ cm}$ along the z axis and $\pm 0.5 \text{ cm}$ in the transverse x - y plane, and a laboratory momentum above $100 \text{ MeV}/c$. Charged kaons and pions are identified based on a likelihood ratio constructed from the specific ionization measurements in the CDC, time-of-flight information from the TOF, and response from the

ACC [46].

Neutral kaon (K_S^0) candidates are reconstructed from pairs of oppositely-charged tracks, treated as pions, and identified by a multivariate analysis [47] based on two sets of input variables [48]. The first set that separates K_S^0 candidates from the combinatorial background are: (1) the K_S^0 momentum in the laboratory frame, (2) the distance along the z axis between the two track helices at their closest approach, (3) the flight length in the x - y plane, (4) the angle between the K_S^0 momentum and the vector joining its decay vertex to the nominal IP, (5) the angle between the π momentum and the laboratory-frame direction of the K_S^0 in its rest frame, (6) the distances of closest approach in the x - y plane between the IP and the pion helices, (7) the numbers of hits for axial and stereo wires in the CDC for each pion, and (8) the presence or absence of associated hits in the SVD for each pion. The second set of variables, which identifies $\Lambda \rightarrow p\pi^-$ background that has a similar long-lived topology, are: (1) particle identification information, momentum, and polar angles of the two daughter tracks in the laboratory frame, and (2) the invariant mass calculated with the proton- and pion-mass hypotheses for the two tracks. In total, the first and second sets comprise 13 and 7 input variables, respectively. The selected K_S^0 candidates are required to have an invariant mass within ± 10 MeV/ c^2 of the nominal value [9], corresponding to a $\pm 3\sigma$ interval in mass resolution, where σ represents the standard deviation.

We reconstruct π^0 candidates from two photons each with energy greater than 50 MeV. We require a minimum momentum of 100 MeV/ c in the CM frame and the invariant mass to

TABLE I. Reconstructed X_s final states [44]. The mode IDs with an asterisk indicate the flavor-non-specific decays which are not used for A_{CP} measurements.

Mode ID	Final state	Mode ID	Final state
1	$K^+\pi^-$	20	$K_S^0\pi^+\pi^0\pi^0$
2	$K_S^0\pi^+$	21	$K^+\pi^+\pi^-\pi^0\pi^0$
3	$K^+\pi^0$	22*	$K_S^0\pi^+\pi^-\pi^0\pi^0$
4*	$K_S^0\pi^0$	23	$K^+\eta$
5	$K^+\pi^+\pi^-$	24*	$K_S^0\eta$
6*	$K_S^0\pi^+\pi^-$	25	$K^+\eta\pi^-$
7	$K^+\pi^-\pi^0$	26	$K_S^0\eta\pi^+$
8	$K_S^0\pi^+\pi^0$	27	$K^+\eta\pi^0$
9	$K^+\pi^+\pi^-\pi^-$	28*	$K_S^0\eta\pi^0$
10	$K_S^0\pi^+\pi^+\pi^-$	29	$K^+\eta\pi^+\pi^-$
11	$K^+\pi^+\pi^-\pi^0$	30*	$K_S^0\eta\pi^+\pi^-$
12*	$K_S^0\pi^+\pi^-\pi^0$	31	$K^+\eta\pi^-\pi^0$
13	$K^+\pi^+\pi^+\pi^-\pi^-$	32	$K_S^0\eta\pi^+\pi^0$
14*	$K_S^0\pi^+\pi^+\pi^-\pi^-$	33	$K^+K^+K^-$
15	$K^+\pi^+\pi^-\pi^-\pi^0$	34*	$K^+K^-K_S^0$
16	$K_S^0\pi^+\pi^+\pi^-\pi^0$	35	$K^+K^+K^-\pi^-$
17	$K^+\pi^0\pi^0$	36	$K^+K^-K_S^0\pi^+$
18*	$K_S^0\pi^0\pi^0$	37	$K^+K^+K^-\pi^0$
19	$K^+\pi^-\pi^0\pi^0$	38*	$K^+K^-K_S^0\pi^0$

TABLE II. Mode category definitions for X_s fragmentation study.

Mode category	Definition	Mode ID
1	$K\pi$ without π^0	1,2
2	$K\pi$ with π^0	3,4
3	$K2\pi$ without π^0	5,6
4	$K2\pi$ with π^0	7,8
5	$K3\pi$ without π^0	9,10
6	$K3\pi$ with π^0	11,12
7	$K4\pi$	13–16
8	$K2\pi^0$	17–22
9	$K\eta$	23–32
10	$3K$	33–38

be within ± 10 MeV/ c^2 of the nominal π^0 mass, corresponding to about 1.5σ in resolution. To reduce the large combinatorial background, we require the cosine of the angle between two photons in the CM frame to be greater than 0.5.

The η candidates are formed from two photons, each with energy greater than 100 MeV. The photon pairs with invariant mass satisfying 515 MeV/ $c^2 < M_{\gamma\gamma} < 570$ MeV/ c^2 , which corresponds to about 2σ in resolution, are retained. We require a CM momentum to be greater than 500 MeV/ c and an absolute value of the cosine of the helicity angle, which is the angle between momentum of one of the photons and direction of laboratory system in the η rest frame, to be less than 0.8.

The 38 X_s final states are reconstructed from the selected π^+ , π^0 , K^+ , K_S^0 , and η candidates. In order to reduce the large combinatorial background from events with high multiplicity, we require $M_{X_s} < 2.8$ GeV/ c^2 , which corresponds to photon energy threshold of about 1.9 GeV. The $K4\pi$ and $K2\pi^0$ mode categories, listed in Table II, have substantial background. Therefore, the momentum of the first and second leading pions (neutral pions) in $K4\pi$ ($K2\pi^0$) category is required to be above 400 MeV/ c and 250 MeV/ c , respectively.

B meson candidates are reconstructed by combining an X_s with a prompt photon candidate. We form two kinematic variables to select B mesons: the energy difference $\Delta E \equiv E_B^{\text{CM}} - E_{\text{beam}}^{\text{CM}}$ and the beam-energy constrained mass $M_{\text{bc}} \equiv \sqrt{(E_{\text{beam}}^{\text{CM}}/c^2)^2 - (\mathbf{p}_B^{\text{CM}}/c)^2}$, where $E_{\text{beam}}^{\text{CM}}$, E_B^{CM} and \mathbf{p}_B^{CM} are the beam energy, energy and momentum of the B candidate in the CM system, respectively. The B momentum vector \mathbf{p}_B^{CM} is calculated without using the magnitude of the photon momentum according to $\mathbf{p}_B^{\text{CM}} = \mathbf{p}_{X_s}^{\text{CM}} + \mathbf{p}_\gamma^{\text{CM}}/|\mathbf{p}_\gamma^{\text{CM}}| \times (E_{\text{beam}}^{\text{CM}} - E_{X_s}^{\text{CM}})$, as the X_s momentum ($\mathbf{p}_{X_s}^{\text{CM}}$) and the beam energy are determined with a substantially better precision than that of the photon candidate. We define the signal region in ΔE and M_{bc} as -0.15 GeV $< \Delta E < 0.08$ GeV and 5.27 GeV/ $c^2 < M_{\text{bc}} < 5.29$ GeV/ c^2 . The ΔE selection is tightened to -0.10 GeV $< \Delta E < 0.05$ GeV for the final states with $2\pi^0$ and $\eta\pi^0$ (mode IDs 17–22, 27, 28, 31 and 32) due to larger combinatorial backgrounds. To determine the signal yield and extract physics observables, we fit to the M_{bc} distribution in the wider range of 5.20 GeV/ $c^2 < M_{\text{bc}} < 5.29$ GeV/ c^2 .

V. BACKGROUND REJECTION

After reconstructing the B meson candidates, two dominant backgrounds still remain: events with D meson decays and continuum $e^+e^- \rightarrow q\bar{q}$ ($q = u, d, s, c$) events.

The events with D meson decays, especially the decay chain $B \rightarrow D^{(*)}\rho^+$ followed by $\rho^+ \rightarrow \pi^+\pi^0$ with a high energy photon from the π^0 , give rise to a peak in the signal region of M_{bc} . In order to suppress this background, a D veto is applied for candidates with $M_{X_s} > 2.0 \text{ GeV}/c^2$. D meson candidates of the major 19 hadronic decay modes are reconstructed with combinations of particles used in the X_s reconstruction. The event is rejected if any of the D meson candidates falls in a veto window around the D meson mass. We set the central value and the width of the veto window depending on the charge of the D candidate and whether or not the D candidate is reconstructed in a mode with a π^0 or η meson: the windows are $1835 < M_{D^0} < 1895 \text{ MeV}/c^2$ and $1840 < M_{D^+} < 1900 \text{ MeV}/c^2$ for the modes without π^0 or η , and $1800 < M_{D^0} < 1905 \text{ MeV}/c^2$ and $1805 < M_{D^+} < 1910 \text{ MeV}/c^2$ for the modes with π^0 or η .

The continuum background is suppressed using a multivariate analysis with an artificial neural network [47], mostly relying on the difference in topology of continuum (jet-like) and $B\bar{B}$ (spherical) events. We use the following variables calculated in the CM frame as input parameters to the neural network: (1) the cosine of the angle between the B meson candidate momentum and the z axis, (2) the likelihood ratio of modified Fox-Wolfram moments [49, 50], (3) the cosine of the angle between the thrust axes of the daughter particles of the B candidate and all other particles in the rest of the event (ROE), (4) the thrust value of particles in the ROE, (5) the sphericity and aplanarity [51] of particles in the ROE, (6) the cosine of the angle between the first sphericity axes of the B candidate and the particles in the ROE, (7) the cosine of the angle between the second sphericity axes of the B candidate and the particles in the ROE, (8) the cosine of the angle between the third sphericity axes of the B candidate and the particles in the ROE, (9) the cosine of the angle between the first sphericity axis of the particles in the event and the z axis, and (10) the signal probability density for the ΔE value. The neural network is trained with signal and $q\bar{q}$ -background MC simulation events with $2.2 \text{ GeV}/c^2 < M_{X_s} < 2.8 \text{ GeV}/c^2$. We obtain a neural network output (\mathcal{O}_{NB}) between -1 and $+1$, which can discriminate the continuum background from signal events. The distribution of \mathcal{O}_{NB} for simulated samples is shown in Fig. 1. The \mathcal{O}_{NB} value is required to be greater than 0.87 in order to maximize the signal significance in the range $2.2 \text{ GeV}/c^2 < M_{X_s} < 2.8 \text{ GeV}/c^2$, in which the continuum background is the most substantial. This selection suppresses about 98.5% of the $q\bar{q}$ background while keeping about 51% of the signal events in the MC simulation study.

VI. BEST CANDIDATES SELECTION

After the background suppression, the average number of B candidates per event is about 1.5 for the signal MC simulation sample. In those events we select the candidate with the largest \mathcal{O}_{NB} . This selection keeps about 89% of the correctly reconstructed signal events while reducing the number of cross-feed events by 45%, based on the MC simulation study. The ratio of the number of correctly reconstructed signal events to the number of cross-feed events plus correctly reconstructed signal events is improved from 0.67 to 0.77. Since the average number of B candidates per event for $B\bar{B}$ background is larger, the best candidate selection suppresses this background to 14%.

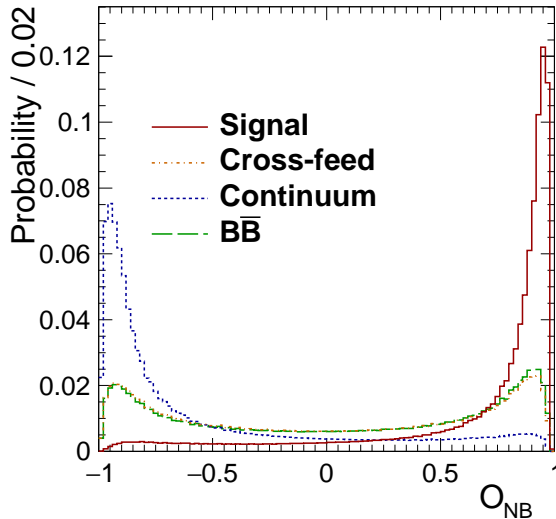


FIG. 1. Neural Network output in simulated data that ranges from -1 for the $q\bar{q}$ background-like events to $+1$ for the signal-like events. The solid (brown) curve shows signal, the dotted-dashed (orange) curve represents cross-feed, the dashed (blue) curve is $q\bar{q}$ background, and the long dashed (green) curve shows $B\bar{B}$ background.

VII. SIGNAL YIELD EXTRACTION

To extract the signal yield and physics observables, we perform a simultaneous fit with an extended unbinned maximum likelihood method to eight M_{bc} distributions; five for B^- , B^+ , \bar{B}^0 , B^0 , and B_{fms} in the on-resonance data, and three for charged B (B^- and B^+), flavor-specific neutral B (\bar{B}^0 and B^0), and B_{fms} in the off-resonance data. Since the off-resonance data only contain continuum background, this is useful to constrain the continuum background shape.

To take into account the run by run difference of beam energy, the M_{bc} value is shifted with $E_{\text{beam}}^{\text{nom}} - E_{\text{beam}}^{\text{run}}$, where $E_{\text{beam}}^{\text{nom}}$ is the nominal beam energy set to 5.289 GeV and $E_{\text{beam}}^{\text{run}}$ is the beam energy for a specific run. By this calibration, the endpoint of the M_{bc} distribution for any run is 5.289 GeV.

The likelihood function consists of probability density functions (PDFs) for signal, cross-feed, peaking and non-peaking background from $B\bar{B}$ events, and $q\bar{q}$ background. All signal and background PDFs are considered for the on-resonance data, while only the $q\bar{q}$ background PDF is used to fit to the off-resonance data. The signal is modeled with a Crystal Ball function [52]:

$$f_{\text{CB}}(x) = \begin{cases} \exp\left(-\frac{1}{2}\left(\frac{x-m}{\sigma_{\text{CB}}}\right)^2\right) & \left(\frac{x-m}{\sigma_{\text{CB}}} \geq -\alpha\right) \\ \frac{\left(\frac{n}{\alpha}\right)^n \exp\left(-\frac{1}{2}\alpha^2\right)}{\left(\frac{n}{\alpha} - \alpha - \frac{x-m}{\sigma_{\text{CB}}}\right)^n} & \left(\frac{x-m}{\sigma_{\text{CB}}} < -\alpha\right), \end{cases}$$

where m and σ_{CB} are the peak position and width, respectively, and the parameters α and n characterize the non-Gaussian tail. The peak position is determined with a large-statistics

$B \rightarrow D\pi$ data sample. The width is obtained from large simulation samples of $B \rightarrow X_s\gamma$ decays corrected for the difference between data and MC simulation decays, which is again obtained using the $B \rightarrow D\pi$ samples. The α and n are fixed to the values obtained from signal MC simulation samples.

For the cross-feed background, we construct five histogram PDFs originating from B^- , B^+ , \bar{B}^0 , B^0 , and B_{fms} with the signal MC simulation sample. The fraction of each cross-feed to the corresponding signal is fixed to the MC simulation value.

A Gaussian function is used to model the peaking background. We consider two types of such backgrounds, originating from π^0 decays and others dominated by η decays. All parameters for the π^0 peaking background are fixed using the events in the sideband defined as $\mathcal{L}_{\pi^0} > 0.5$ and $\mathcal{L}_\eta < 0.2$. The parameters for other peaking background are fixed with the $B\bar{B}$ background MC simulation samples.

The non-peaking background from $B\bar{B}$ events is modeled with an ARGUS function [53]:

$$f_{\text{ARG}}(x) = x \left\{ 1 - \left(\frac{x}{E_{\text{beam}}^{\text{CM}}} \right)^2 \right\}^{1/2} \exp \left[c \left\{ 1 - \left(\frac{x}{E_{\text{beam}}^{\text{CM}}} \right)^2 \right\} \right],$$

where $E_{\text{beam}}^{\text{CM}}$ is fixed to 5.289 GeV and other shape parameters are determined from the MC simulation. The yields for charged B and neutral B are constrained from the on-resonance and scaled off-resonance events in the sideband defined as $M_{\text{bc}} < 5.27$ GeV, separately.

For the $q\bar{q}$ background PDF, we use a modified ARGUS function:

$$f_{\text{ARG}}^{\text{mod}}(x) = x \left\{ 1 - \left(\frac{x}{E_{\text{beam}}^{\text{CM}}} \right)^2 \right\}^p \exp \left[c_{\text{mod}} \left\{ 1 - \left(\frac{x}{E_{\text{beam}}^{\text{CM}}} \right)^2 \right\} \right],$$

where a power parameter, p , is introduced to account for the steep slope at low M_{bc} . The c_{mod} parameter is common for on- and off-resonance data and floated in the fit. The p parameter is fixed from the $q\bar{q}$ MC simulation samples calibrated with the off-resonance data.

There are in total 16 free parameters in the simultaneous fit: five signal yields for the five B categories, eight $q\bar{q}$ yields (five for on-resonance and three for off-resonance), and three c_{mod} shape parameters for $q\bar{q}$. Finally, the physics parameters to be extracted can be written in terms of the efficiency corrected signal yields (N_i) as:

$$\begin{aligned} \Delta_{0-} &= \frac{\frac{\tau_{B^+}}{\tau_{B^0}} \frac{f_{+-}}{f_{00}} (N_{\bar{B}^0} + N_{B^0} + N_{B_{\text{fms}}}) - (N_{B^-} + N_{B^+})}{\frac{\tau_{B^+}}{\tau_{B^0}} \frac{f_{+-}}{f_{00}} (N_{\bar{B}^0} + N_{B^0} + N_{B_{\text{fms}}}) + (N_{B^-} + N_{B^+})}, \\ A_{CP}^C &= \frac{N_{B^-} - N_{B^+}}{N_{B^-} + N_{B^+}}, \\ A_{CP}^N &= \frac{N_{\bar{B}^0} - N_{B^0}}{N_{\bar{B}^0} + N_{B^0}}, \\ A_{CP}^{\text{tot}} &= \frac{(N_{B^-} + N_{\bar{B}^0}) - (N_{B^+} + N_{B^0})}{(N_{B^-} + N_{\bar{B}^0}) + (N_{B^+} + N_{B^0})}, \end{aligned} \quad (5)$$

where A_{CP}^N , A_{CP}^C and A_{CP}^{tot} are direct CP violation parameters for neutral, charged and combined $B \rightarrow X_s\gamma$ decays, τ_{B^+}/τ_{B^0} is the lifetime ratio fixed to the PDG value [9], and f_{+-}/f_{00} is the production ratio of B^+B^- to $B^0\bar{B}^0$ from $\Upsilon(4S)$ decays also fixed to the PDG value [9] [54]. The fitting procedure is validated using the full MC simulation samples and an ensemble test based on toy MC simulation samples.

VIII. CALIBRATION OF X_s FRAGMENTATION MODEL

Since the signal efficiency depends on specific decay modes, the fragmentation model in the inclusive MC simulation is calibrated to that of the data to reduce the systematic uncertainties associated to modeling. The final states are divided into ten categories, defined in Table II, and four M_{X_s} regions are defined ($[1.15,1.5]\text{GeV}/c^2$, $[1.5,2.0]\text{GeV}/c^2$, $[2.0,2.4]\text{GeV}/c^2$ and $[2.4,2.8]\text{GeV}/c^2$) to calibrate the fragmentation model. We adopt the same calibration method as described in Ref. [6].

IX. SYSTEMATIC UNCERTAINTIES

We evaluate the systematic uncertainties associated with particle detection efficiencies, charge asymmetries in particle detection, selections, physics parameters, X_s fragmentation model, background A_{CP} and Δ_{0-} , fixed parameters in the fit, fitter bias, and MC simulation statistics. We list the systematic uncertainties in Table III.

We estimate the tracking efficiency uncertainty using partially reconstructed $D^{*+} \rightarrow D^0\pi^+$, $D^0 \rightarrow K_S^0\pi^+\pi^-$ events. The uncertainties due to kaon and pion identifications are evaluated with clean kaon and pion samples in $D^{*+} \rightarrow D^0\pi^+$, followed by $D^0 \rightarrow K^-\pi^+$. We determine the uncertainty due to π^0 reconstruction by taking the ratio of the efficiencies of $\eta \rightarrow 3\pi^0$ to $\eta \rightarrow \pi^+\pi^-\pi^0$ or $\eta \rightarrow \gamma\gamma$. The uncertainty due to K_S^0 reconstruction is evaluated by checking the efficiency of $K_S^0 \rightarrow \pi^+\pi^-$ as functions of flight length, transverse momentum of K_S^0 , and polar angle of K_S^0 .

We measure the charged-pion detection asymmetry using reconstructed $B \rightarrow X_s\gamma$ candidates (with charged pion in the final state) in the sideband defined as $\mathcal{O}_{\text{NB}} < 0$. The charged kaon detection asymmetry is measured using a large clean kaon sample from $D^0 \rightarrow K^-\pi^+$ decay, where the pion detection asymmetry in the decay is subtracted with pions from $D_s^+ \rightarrow \phi\pi^+$ decays [56].

The uncertainty due to possible mismodeling of the ΔE distribution we estimate by inflating the ΔE width and shifting the mean value.

We evaluate the uncertainties due to f_{+-}/f_{00} and lifetime ratio by changing these values by $\pm 1\sigma$ from the nominal PDG values [9].

The uncertainty due to the fragmentation model we determine by varying the decay channel proportions by their respective uncertainties. The exceptions are the proportions for $K4\pi$ and $K2\pi^0$ in $2.0\text{GeV}/c^2 < M_{X_s} < 2.4\text{GeV}/c^2$ and all the modes in $2.4\text{GeV}/c^2 < M_{X_s} < 2.8\text{GeV}/c^2$, where we use the proportions in MC simulation and a variation of $\pm 50\%$ as uncertainty. The fragmentation uncertainties for each M_{X_s} bin are obtained by summing in quadrature the changes for each of the ten mode categories.

Since the threshold between K^* and the inclusive X_s used in the MC simulation is fixed at $1.15\text{GeV}/c^2$, we change this boundary to $1.10\text{GeV}/c^2$ and $1.20\text{GeV}/c^2$ to evaluate the uncertainty due to the threshold.

The proportion of missing final states that are not included in our reconstructed modes affects the reconstruction efficiency. We evaluate the uncertainty on the relative proportion of each of the 38 measured final states by varying the parameters of the fragmentation model used in the calibration of the MC simulation within their allowed ranges as determined from data. We take the difference from the nominal value as the systematic uncertainty on the missing fraction.

We evaluate the uncertainties due to A_{CP} and Δ_{0-} in the background decays by changing the A_{CP} and Δ_{0-} values by $\pm 1\sigma$ from the nominal PDG values [9]; if neither A_{CP} nor Δ_{0-} are measured, we assign $\pm 100\%$ uncertainties.

We evaluate the uncertainties due to tail parameters, α and n , in the signal PDF by floating in turn each of the fixed shape parameters in the fit while fixing the other shape parameters to their nominal values. Then the two uncertainties are added in quadrature. Since the α and n are anti-correlated, this procedure conservatively estimates the uncertainties. The uncertainties due to the other fixed parameters in the signal PDF are evaluated by varying them by $\pm 1\sigma$ from the nominal values. The uncertainty due to cross-feed is caused by two sources; one is multiplicity of hadrons in the other B meson decays, the other is fragmentation model for signal. Both changes the shape and yield of cross-feed. The former is evaluated with MC simulation by changing the multiplicities of π^\pm , π^0 , K^\pm , K^0 and η in the other B meson decays MC simulation from the nominal values to PDG values taking into account their uncertainties [9]. The latter is determined with MC simulation by varying the decay channel proportions by their respective uncertainties. We estimate the uncertainty due to the p parameter in $q\bar{q}$ background PDF by changing the parameter by $\pm 1\sigma$ as obtained from the fit to the off-resonance data. To evaluate the uncertainty due to the peaking background from π^0 decays, we vary the parameter values by $\pm 1\sigma$ as determined from the sideband data. The systematic uncertainties of other peaking backgrounds, which are subleading to the π^0 backgrounds, we evaluate by changing the normalizations by $\pm 20\%$ which is about twice larger than the uncertainties of the corresponding branching fractions.

We check for possible bias in the fit by performing a large number of pseudo-experiments. In the study, we observe small biases which we add to the systematic uncertainty.

We also take into account the statistical uncertainty of the efficiency estimated with MC simulation samples as systematic uncertainty.

The systematic uncertainties due to efficiencies and background Δ_{0-} are only relevant for Δ_{0-} and A_{CP}^{tot} since these cancel out by taking the CP asymmetry in the other observables. The systematic uncertainties due to physics parameters to convert the signal yields to decay widths are only relevant for Δ_{0-} . The systematic uncertainties due to charged particle detection asymmetry and background A_{CP} are only relevant for A_{CP} as they cancel out for the CP -averaged observable Δ_{0-} . The largest and dominant systematic uncertainty for Δ_{0-} is due to f_{+-}/f_{00} . The dominant systematic sources for ΔA_{CP} and A_{CP} are due to peaking background from π^0 decays and charge asymmetries in particle detection.

X. RESULTS

We perform a simultaneous fit to eight M_{bc} distributions shown in Figure 2, with the PDFs as described above, to extract the following results

$$\begin{aligned}
 \Delta_{0-} &= (-0.48 \pm 1.49 \pm 0.97 \pm 1.15)\%, \\
 \Delta A_{CP} &= (+3.69 \pm 2.65 \pm 0.76)\%, \\
 A_{CP}^C &= (+2.75 \pm 1.84 \pm 0.32)\%, \\
 A_{CP}^N &= (-0.94 \pm 1.74 \pm 0.47)\%, \\
 A_{CP}^{\text{tot}} &= (+1.44 \pm 1.28 \pm 0.11)\%, \\
 \bar{A}_{CP} &= (+0.91 \pm 1.21 \pm 0.13)\%,
 \end{aligned}$$

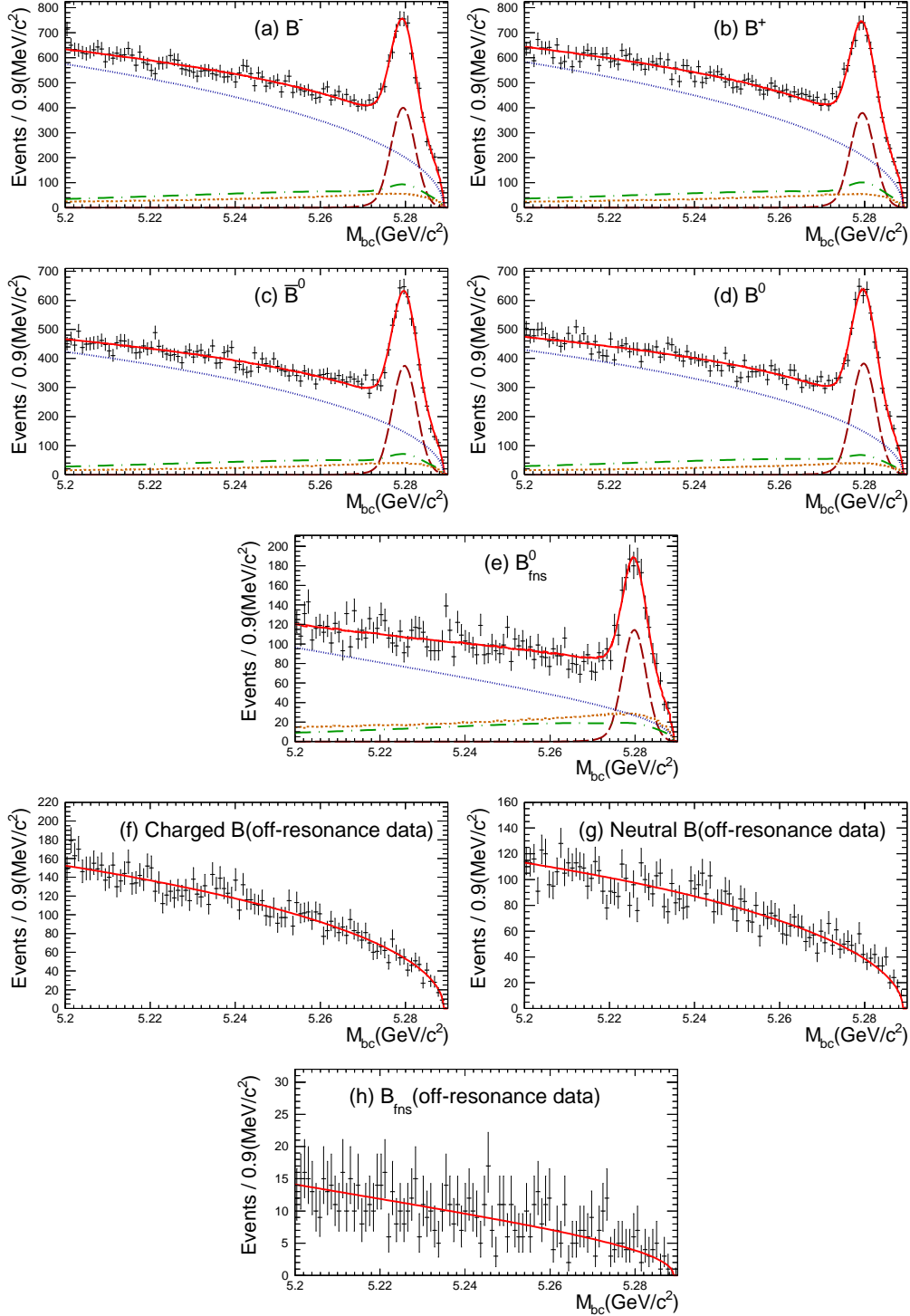


FIG. 2. M_{bc} distributions for (a) B^- , (b) B^+ , (c) \bar{B}^0 , (d) B^0 , and (e) B_{fns}^0 in on-resonance data, and (f) charged B , (g) neutral B and (h) B_{fns} in off-resonance data. The points with error bars show the data and the lines show different contributions as obtained from the fit. The long dashed (brown) curves represent signal, the dotted (blue) curves show continuum, the dotted-dashed (green) curves are $B\bar{B}$ background, the dashed (orange) curves show cross-feed, and solid (red) curves are the sum of all contributions.

TABLE III. Absolute systematic uncertainties for Δ_{0-} , ΔA_{CP} and A_{CP} in percent.

Source	Δ_{0-}	ΔA_{CP}	A_{CP}^C	A_{CP}^N	A_{CP}^{tot}	\bar{A}_{CP}
tracking	± 0.02	–	–	–	< 0.01	–
K/π ID	± 0.05	–	–	–	< 0.01	–
π^0/η recon.	± 0.01	–	–	–	< 0.01	–
K_S^0 recon.	± 0.01	–	–	–	< 0.01	–
detection asym.	–	± 0.39	± 0.11	± 0.29	± 0.05	± 0.10
ΔE selection	$+0.03$ -0.06	–	–	–	< 0.01	–
f_{+-}/f_{00}	± 1.15	–	–	–	–	–
lifetime ratio	± 0.19	–	–	–	–	–
fragmentation	± 0.58	–	–	–	± 0.01	–
K^*-X_s transition	± 0.13	–	–	–	< 0.01	–
missing fraction	± 0.02	–	–	–	< 0.01	–
background A_{CP}	–	± 0.04	± 0.03	± 0.04	± 0.02	± 0.02
background Δ_{0-}	± 0.01	–	–	–	< 0.01	–
fixed parameters	$+0.74$ -0.65	$+0.64$ -0.61	$+0.30$ -0.28	$+0.34$ -0.36	± 0.07	$+0.07$ -0.06
fitter bias	$+0.08$ -0.07	$+0.11$ -0.07	$+0.04$ -0.00	$+0.10$ -0.09	$+0.05$ -0.02	$+0.06$ -0.03
MC sim. stat.	± 0.03	–	–	–	< 0.01	–
total	$+1.51$ -1.47	$+0.76$ -0.73	$+0.32$ -0.30	$+0.46$ -0.47	$+0.11$ -0.09	$+0.13$ -0.12

where the first uncertainty is statistical, the second is systematic, and the third for Δ_{0-} is due to f_{+-}/f_{00} . The fit results for the signal yields are summarized in Table IV. The correlation matrix of the six observables is given in Table V. The χ^2 and number of degrees of freedom in the simultaneous fit calculated from the data points and fit curves in Fig. 2 are 728 and 784, respectively. The measured Δ_{0-} is consistent with zero and the precision is better than that of BaBar by a factor of three [37]. Thus, this measurement can be used to constrain the resolved photon contribution in $B \rightarrow X_s \gamma$ as

$$\frac{\mathcal{B}_{\text{RP}}^{78}}{\mathcal{B}} \simeq (+0.16 \pm 0.50 \pm 0.32 \pm 0.38 \pm 0.05)\%,$$

where the last uncertainty is associated with $SU(3)$ flavor-symmetry breaking. This result improves the prediction of the branching fraction. The result for ΔA_{CP} is consistent with zero, as predicted in the SM, thus the measurement can be used to constrain NP models, for example, in the supersymmetry model described in Ref. [36], this excludes the parameter space for squark mass below $5.0 \text{ TeV}/c^2$.

We checked M_{X_s} dependences of the observables and find no dependences except Δ_{0-} in K^* mass region is larger than the measurement and is consistent with the world average [9].

XI. CONFIDENCE LEVEL INTERVALS

From our measurement of ΔA_{CP} , we set confidence intervals on $\text{Im}(C_8/C_7)$ based on Eq. (4). The hadronic parameter $\tilde{\Lambda}_{78}$ has a large uncertainty and the range is estimated as $17 \text{ MeV} < \tilde{\Lambda}_{78} < 190 \text{ MeV}$ with a vacuum insertion approximation [33]. Since an uncertainty

TABLE IV. Signal yields (N_S) and efficiencies (ϵ). The uncertainties for N_S are statistical. The uncertainties for ϵ include systematic uncertainties.

Mode	N_S	ϵ [%]
B^-	3243 ± 85	2.21 ± 0.12
B^+	3074 ± 86	2.23 ± 0.12
\bar{B}^0	3038 ± 78	2.42 ± 0.14
B^0	3102 ± 79	2.46 ± 0.14
B_{fns}	902 ± 42	0.375 ± 0.023

TABLE V. The correlation matrix for the six observables.

	Δ_{0-}	ΔA_{CP}	A_{CP}^C	A_{CP}^N	A_{CP}^{tot}	\bar{A}_{CP}
Δ_{0-}	1.00	0.07	0.06	-0.05	-0.01	0.01
ΔA_{CP}	0.07	1.00	0.70	-0.68	0.29	0.03
A_{CP}^C	0.06	0.70	1.00	-0.12	0.91	0.74
A_{CP}^N	-0.05	-0.68	-0.12	1.00	0.47	0.72
A_{CP}^{tot}	-0.01	0.29	0.91	0.47	1.00	0.94
\bar{A}_{CP}	0.01	0.03	0.74	0.72	0.94	1.00

of $\tilde{\Lambda}_{78}$ is hard to estimate, we set the 1σ and 2σ confidence level intervals for $\text{Im}(C_8/C_7)$ as a function of $\tilde{\Lambda}_{78}$ within the range described above as shown in Figure 3. Our result constrains $\text{Im}(C_8/C_7)$ in the positive region better than the only previously available measurement from BaBar [32], and gives a strong constraint on NP models [36]. If we take the average value of $\tilde{\Lambda}_{78} = 89$ MeV as a benchmark [35], the 2σ confidence intervals is $-0.17 < \text{Im}(C_8/C_7) < 0.86$.

XII. CONCLUSION

In summary, we have measured the isospin asymmetry and the difference of the direct CP asymmetries between charged and neutral $B \rightarrow X_s \gamma$ decays with a sum-of-exclusive technique based on a sample of 772×10^6 $B\bar{B}$ pairs with an assumption that the observables have no dependence on the specific decay modes nor on M_{X_s} . The measurement of Δ_{0-} is consistent with zero and can constrain the resolved photon contribution in $B \rightarrow X_s \gamma$, which will improve the prediction of the branching fraction. The result of ΔA_{CP} is consistent with zero as predicted in the SM, enabling constraints on NP models. Our measurements of the CP asymmetries are consistent with zero, and also with the SM predictions. All the results are the most precise to date and will be useful for constraining the parameter space in NP models. Current A_{CP} and ΔA_{CP} measurements are dominated by the statistical uncertainty; thus, the upcoming Belle II experiment will further reduce the uncertainty. To improve the isospin asymmetry at Belle II, reduction of the dominant uncertainty due to f_{+-}/f_{00} is essential, and can be performed at both Belle and Belle II.

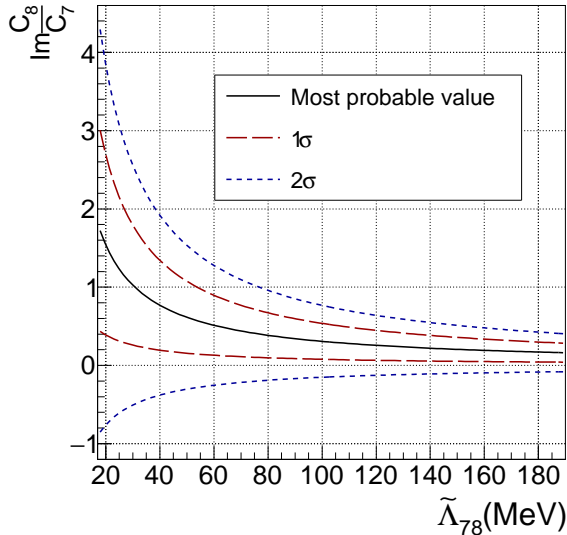


FIG. 3. The solid (black), dashed (red) and dotted (blue) curves show the most probable value, 1σ and 2σ confidence intervals for $\text{Im}(C_8/C_7)$ as a function of $\tilde{\Lambda}_{78}$, respectively. The range of $\tilde{\Lambda}_{78}$ is chosen to be $17\text{MeV} < \tilde{\Lambda}_{78} < 190\text{MeV}$.

ACKNOWLEDGMENTS

Authors would like to thank M. Misiak, G. Paz and M. Endo for fruitful discussions. A. I. is supported by the Japan Society for the Promotion of Science (JSPS) Grant No. 16H03968. We thank the KEKB group for the excellent operation of the accelerator; the KEK cryogenics group for the efficient operation of the solenoid; and the KEK computer group, the National Institute of Informatics, and the Pacific Northwest National Laboratory (PNNL) Environmental Molecular Sciences Laboratory (EMSL) computing group for valuable computing and Science Information NETwork 5 (SINET5) network support. We acknowledge support from the Ministry of Education, Culture, Sports, Science, and Technology (MEXT) of Japan, the Japan Society for the Promotion of Science (JSPS), and the Tau-Lepton Physics Research Center of Nagoya University; the Australian Research Council; Austrian Science Fund under Grant No. P 26794-N20; the National Natural Science Foundation of China under Contracts No. 11435013, No. 11475187, No. 11521505, No. 11575017, No. 11675166, No. 11705209; Key Research Program of Frontier Sciences, Chinese Academy of Sciences (CAS), Grant No. QYZDJ-SSW-SLH011; the CAS Center for Excellence in Particle Physics (CCEPP); Fudan University Grant No. JIH5913023, No. IDH5913011/003, No. JIH5913024, No. IDH5913011/002; the Ministry of Education, Youth and Sports of the Czech Republic under Contract No. LTT17020; the Carl Zeiss Foundation, the Deutsche Forschungsgemeinschaft, the Excellence Cluster Universe, and the VolkswagenStiftung; the Department of Science and Technology of India; the Istituto Nazionale di Fisica Nucleare of Italy; National Research Foundation (NRF) of Korea Grants No. 2014R1A2A2A01005286, No.2015R1A2A2A01003280, No. 2015H1A2A1033649, No. 2016R1D1A1B01010135, No. 2016K1A3A7A09005 603, No. 2016R1D1A1B02012900; Radiation Science Research Institute, Foreign Large-size Research Facility Application Supporting project and the Global Science Experimental Data Hub Center of the Korea

Institute of Science and Technology Information; the Polish Ministry of Science and Higher Education and the National Science Center; the Ministry of Education and Science of the Russian Federation and the Russian Foundation for Basic Research; the Slovenian Research Agency; Ikerbasque, Basque Foundation for Science, Basque Government (No. IT956-16) and Ministry of Economy and Competitiveness (MINECO) (Juan de la Cierva), Spain; the Swiss National Science Foundation; the Ministry of Education and the Ministry of Science and Technology of Taiwan; and the United States Department of Energy and the National Science Foundation.

- [1] S. Chen *et al.* (CLEO Collaboration), Phys. Rev. Lett. **87**, 251807 (2001).
- [2] B. Aubert *et al.* (BaBar Collaboration), Phys. Rev. D **77**, 051103 (2008).
- [3] J. P. Lees *et al.* (BaBar Collaboration), Phys. Rev. Lett. **109**, 191801 (2012).
- [4] J. P. Lees *et al.* (BaBar Collaboration), Phys. Rev. D **86**, 052012 (2012).
- [5] A. Limosani *et al.* (Belle Collaboration), Phys. Rev. Lett. **103**, 241801 (2009).
- [6] T. Saito *et al.* (Belle Collaboration), Phys. Rev. D **91**, 052004 (2015).
- [7] M. Misiak *et al.*, Phys. Rev. Lett. **114**, 221801 (2015).
- [8] See, for example, U. Haisch and A. Weiler, Phys. Rev. D **76**, 034014 (2007); A. Freitas and U. Haisch, Phys. Rev. D **77**, 093008 (2008); M. Blanke, A. J. Buras, K. Gemmler and T. Heidsieck, J. High Energy Phys. 03 (2012) 024; K. Ishiwata, N. Nagata and N. Yokozaki, Phys. Lett. B **710**, 145 (2012); W. Altmannshofer, M. Carena, N. R. Shah and F. Yu, J. High Energy Phys. 01 (2013) 160; A. Katz, M. Reece and A. Sajjad, J. High Energy Phys. 10 (2014) 102; H. Baer, V. Barger, N. Nagata and M. Savoy, Phys. Rev. D **95**, 055012 (2017); M. Misiak and M. Steinhauser, Eur. Phys. J. C **77**, 201 (2017).
- [9] M. Tanabashi *et al.* (Particle Data Group), Phys. Rev. D **98**, 030001 (2018).
- [10] E. Kou *et al.*, “The Belle II Physics book,” chapter 9 “Radiative and Electroweak Penguin B Decays”, arXiv:1808.10567 [hep-ex], submitted to Prog. Theor. Exp. Phys.
- [11] S. J. Lee, M. Neubert and G. Paz, Phys. Rev. D **75**, 114005 (2007).
- [12] M. Misiak, Acta Phys. Polon. B **40**, 2987 (2009).
- [13] M. Benzke, S. J. Lee, M. Neubert and G. Paz, J. High Energy Phys. 08 (2010) 099.
- [14] T. Horiguchi *et al.* (Belle Collaboration), Phys. Rev. Lett. **119**, 191802 (2017).
- [15] A. L. Kagan and M. Neubert, Phys. Lett. B **539**, 227 (2002).
- [16] M. Matsumori, A. I. Sanda and Y. Y. Keum, Phys. Rev. D **72**, 014013 (2005).
- [17] P. Ball, G. W. Jones and R. Zwicky, Phys. Rev. D **75**, 054004 (2007).
- [18] M. Jung, X. Q. Li and A. Pich, J. High Energy Phys. 10 (2012) 063.
- [19] M. Ahmady and R. Sandapen, Phys. Rev. D **88**, 014042 (2013).
- [20] J. Lyon and R. Zwicky, Phys. Rev. D **88**, 094004 (2013).
- [21] L. Wolfenstein and Y. L. Wu, Phys. Rev. Lett. **73**, 2809 (1994).
- [22] H. M. Asatrian and A. N. Ioannissian, Phys. Rev. D **54**, 5642 (1996).
- [23] A. L. Kagan and M. Neubert, Phys. Rev. D **58**, 094012 (1998).
- [24] C. K. Chua, X. G. He and W. S. Hou, Phys. Rev. D **60**, 014003 (1999).
- [25] K. Kiers, A. Soni and G. H. Wu, Phys. Rev. D **62**, 116004 (2000)
- [26] H. H. Asatryan, H. M. Asatrian, G. K. Yeghiyan and G. K. Savvidy, Int. J. Mod. Phys. A **16**, 3805 (2001).
- [27] T. Hurth, E. Lunghi and W. Porod, Nucl. Phys. B **704**, 56 (2005).

- [28] R. Barbieri, P. Campli, G. Isidori, F. Sala and D. M. Straub, *Eur. Phys. J. C* **71**, 1812 (2011)
- [29] Y. Shimizu, M. Tanimoto and K. Yamamoto, *Prog. Theor. Phys.* **128**, 273 (2012).
- [30] A. Arbey, J. Ellis, R. M. Godbole and F. Mahmoudi, *Eur. Phys. J. C* **75**, 85 (2015).
- [31] S. Nishida *et al.* (Belle Collaboration), *Phys. Rev. Lett.* **93**, 031803 (2004).
- [32] J. P. Lees *et al.* (BaBar Collaboration), *Phys. Rev. D* **90**, 092001 (2014).
- [33] M. Benzke, S. J. Lee, M. Neubert and G. Paz, *Phys. Rev. Lett.* **106**, 141801 (2011).
- [34] For the definition of the Wilson coefficients and these operators, see for example, M. Czakon, P. Fiedler, T. Huber, M. Misiak, T. Schutzmeier and M. Steinhauser, *J. High Energy Phys.* 04 (2015) 168.
- [35] R. Malm, M. Neubert and C. Schmell, *J. High Energy Phys.* 04 (2016) 042.
- [36] M. Endo, T. Goto, T. Kitahara, S. Mishima, D. Ueda and K. Yamamoto, *J. High Energy Phys.* 04 (2018) 019.
- [37] B. Aubert *et al.* (BaBar Collaboration), *Phys. Rev. D* **72**, 052004 (2005).
- [38] A. Abashian *et al.* (Belle Collaboration), *Nucl. Instrum. Methods Phys. Res., Sect. A* **479**, 117 (2002); also see detector section in J. Brodzicka *et al.*, *Prog. Theor. Exp. Phys.* **2012**, 04D001 (2012).
- [39] S. Kurokawa and E. Kikutani, *Nucl. Instrum. and Methods Phys. Res., Sect. A* **499**, 1 (2003), and other papers included in this volume.
- [40] D. J. Lange, *Nucl. Instrum. Methods Phys. Res., Sect. A* **462**, 152 (2001).
- [41] R. Brun *et al.*, GEANT, CERN Report No. DD/EE/84-1 (1984).
- [42] A. L. Kagan and M. Neubert, *Eur. Phys. J. C* **7**, 5 (1999).
- [43] T. Sjöstrand, S. Mrenna and P. Skands, *J. High Energy Phys.* 05 (2006) 026.
- [44] Throughout this paper, the inclusion of the charge conjugate mode decay is implied unless otherwise stated.
- [45] P. Koppenburg *et al.* (Belle Collaboration), *Phys. Rev. Lett.* **93**, 061803 (2004).
- [46] E. Nakano, *Nucl. Instrum. Methods Phys. Res., Sect. A* **494**, 402 (2002).
- [47] NeuroBayes software package based on Bayesian statistics, in M. Feindt and U. Kerzel, *Nucl. Instrum. Methods Phys. Res., Sect. A* **559**, 190 (2006).
- [48] H. Nakano, Ph.D Thesis, Tohoku University (2014) Chapter 4, unpublished, https://tohoku.repo.nii.ac.jp/?action=pages_view_main&active_action=repository_view_main_item_detail&item_id=70563&item_no=1&page_id=33&block_id=38.
- [49] The Fox-Wolfram moments were introduced in G. C. Fox and S. Wolfram, *Phys. Rev. Lett.* **41**, 1581 (1978).
- [50] S. H. Lee *et al.* (Belle Collaboration), *Phys. Rev. Lett.* **91**, 261801 (2003).
- [51] J. D. Bjorken and S. J. Brodsky, *Phys. Rev. D* **1**, 1416 (1970).
- [52] T. Skwarnicki, Ph.D. Thesis, Institute for Nuclear Physics, Krakow 1986; DESY Internal Report, DESY F31-86-02 (1986).
- [53] H. Albrecht *et al.* (ARGUS Collaboration), *Phys. Lett. B* **241**, 278 (1990).
- [54] There is a discussion on the production ratio f_{+-}/f_{00} given by the PDG, M. Jung, *Phys. Lett. B* **753**, 187 (2016). A. Ishikawa found a miscalculation in the update of the Belle result [55] with the latest physics parameters and M. Jung confirmed this. The erratum is expected to be published.
- [55] N. C. Hastings *et al.* (Belle Collaboration), *Phys. Rev. D* **67**, 052004 (2003).
- [56] B. R. Ko *et al.* (Belle Collaboration), *J. High Energy Phys.* 02 (2013) 098.